Micro-SQUIDs with controllable asymmetry via hot-phonon controlled junctions

G. J. Podd,[1,][*] G. D. Hutchinson,[2] D. A. Williams,[2] and D. G. Hasko[1]

[1]*Microelectronics Research Centre, Cavendish Laboratory, University of Cambridge, Cambridge CB3 0HE, United Kingdom*
[2]*Hitachi Cambridge Laboratory, Hitachi Europe Ltd., Cambridge CB3 0HE, United Kingdom*
(Received 6 December 2006; published 2 April 2007)

We describe the fabrication and measurement of a micrometer-sized direct-current superconducting quantum interference device (dc-SQUID) in which the critical currents of each of the constriction-type Josephson junctions can be controlled independently and *in situ* via a process of nonequilibrium (hot-phonon) irradiation from a nanofabricated gated structure. The control mechanism is based on hot phonons which are injected into the superconducting microbridges from close proximity, but electrically isolated, normal-metal constrictions. We have also developed a one-dimensional computer model to analyze the behavior of micro-SQUID devices including situations in which we modify the asymmetry of the device. We show from the model that the experimental results are consistent with a change in effective length of the microbridge junctions with respect to the coherence length of the film. The experimental data, and its interpretation in relation to the micro-SQUID model, confirm that this technique, based on hot-phonon irradiation for controlling the critical current in Dayem bridge Josephson junctions, is compatible with the Josephson effect and a feasible method for post-fabrication parameter control in superconducting circuits using Dayem bridge Josephson junctions.

PACS number(s): 74.62.Yb, 85.25.Dq

I. INTRODUCTION

The macroscopic quantum nature of the superconducting state gives rise to a number of phenomena that can be exploited in superconductor devices. Two of these are the Josephson effect and flux quantization in units of the flux quantum $\Phi_0 = 2.07 \times 10^{-15}$ Wb in a region enclosed by a superconductor. These two properties are combined in the direct-current superconducting quantum interference device (dc-SQUID) since the dc-SQUID consists of a superconducting loop interrupted by two Josephson junctions and the critical current of the device is periodic in the applied magnetic flux. The period of the oscillations of the device is given by the flux quantum, which makes them highly sensitive magnetic flux sensors. The result of this is that they have found applications in wide variety of areas from biomagnetism to geophysical measurements.[1]

The micro-SQUID is particular type of dc-SQUID with a loop area of the order of 1 μm^2 and was developed in order to study the magnetic response of small samples.[2] The micro-SQUID device with constant-thickness bridges was first fabricated by Chapelier *et al.*[3] in aluminum using a single electron-beam lithographic step and subsequent aluminum evaporation. By fabricating Dayem bridge Josephson junctions with characteristic dimensions of the order of 100 nm in a micrometer-sized superconducting loop, the micro-SQUID is ideal for making local magnetic measurements due to the devices insensitivity to in-plane background magnetic fluctuations (typically the critical current oscillations have a period of a few mT). As a result of these properties micro-SQUIDs have been used in a variety of applications including the detection of magnetization reversal in nanoscale magnetic particles,[4–6] the magnetic response of a mesoscopic GaAs ring,[7] and for a scanning micro-SQUID microscope.[2,8] Another proposed application has been as an element in a magnetic qubit architecture for quantum computing.[9] Recent developments have seen the development of even smaller structures such as the nano-SQUID,[10] which consists of a 200-nm hole with the aim to detect small spin populations[11] or the creation of single-photon detectors.[12]

In addition to the small loop area, the key component of a micro-SQUID device that distinguishes it from other dc-SQUID structures is the Dayem bridge Josephson junction.[13] Conventionally dc-SQUIDs tend to employ tunnel junctions; however, these are incompatible with the small loop size used for micro-SQUIDs, since in a dc-SQUID it is desirable that the device satisfy the relationship $2LI_C/\Phi_0 \sim 1$ for optimum performance.[14] Tunnel junctions have low critical current densities, which means that in the low inductance limit of the small-looped micro-SQUID they do not satisfy this criterion, whereas the large critical current densities of Dayem bridge junctions mean they are more suited to fulfilling the condition. The Dayem bridge Josephson junction consists of a constriction in the superconductor with weak current concentration[15] which causes it to act as a weak link with Josephson properties. The advantage of the Dayem bridge or microbridge junction is that it are relatively easy to fabricate in a micro-SQUID configuration either by electron beam lithography[3] or by scanning probe techniques.[16,17]

In this paper we investigate the technique of critical current control in Dayem bridge Josephson junctions, which has been previously investigated with a variety of Josephson junction types and with a variety of gating techniques. These include the four-terminal voltage-controlled superconductor-normal-superconductor type (SNS) Josephson junction[18,19] and the superconductor-semiconductor-superconductor junctions utilizing current injection,[20,21] as well as structures using high-mobility two-dimensional electron gas (2DEG) heterostructures, which incorporate surface gating.[22,23] The control of dc-SQUID characteristics post-fabrication, using the four-terminal voltage-controlled SNS Josephson junction, has been demonstrated[24,25] with the ability to modify the critical currents of the junctions including the reversal of the supercurrent in the junction.

The method shown to be compatible with the Josephson effect in Dayem bridge structures is the technique of critical current control via hot-phonon irradiation.[26–30] The technique was first used on a superconducting bridge to demonstrate a superconducting nanotransistor in which a significant voltage gain could be achieved at liquid helium temperatures. Here a close proximity, but electrically isolated, normal-metal constriction injected nonequilibrium phonons in a process driven by the application of a voltage. The phonons reduced the critical current of the device by breaking the Cooper pairs in the superconductor and thus weakened the superconducting state in the vicinity of the constriction. The control mechanism was then shown to be compatible with the Josephson effect—that is, it did not destroy the phase coherence of the junctions—by the development of a controllable micro-SQUID device in which hot-phonon irradiation on both junctions in a nonindependent way was used to adjust the critical current of the dc-SQUID in an electrically isolated process.[31,32]

This paper presents the implementation of independent hot-phonon control upon each of the two superconducting constriction-type junctions that form the Josephson elements of a micro-SQUID in order to control the asymmetry of the device post-fabrication. The asymmetry of a dc-SQUID can be a manifestation of a difference in the inductance between the two arms of the device: the shunt resistance of the junctions and the critical currents of the junctions.[14,33] The asymmetric inductance case has been investigated previously in the case of a dc-SQUID as an amplifier,[34] and an asymmetry was found to increase the current gain. Testa *et al.*[35] have modeled and tested dc-SQUIDs in which the shunt resistance of the two junctions is different, superconducting quantum interference device asymmetric (shunt) resistance (SQUIDARs), and they found advantages in an improved flux to voltage transfer coefficient over standard symmetric dc-SQUIDs. Critical-current asymmetric dc-SQUIDs have been fabricated in which the junctions are of the SNS type[36] and the critical current of the junctions was controlled by the electron temperature within the junction with the view towards applications in sensitive particle detectors.

By presenting our experiments we describe in detail a fabrication procedure to create the independently controlled micro-SQUID. We then show the results of our measurements of this device, and by having separate control wires for each junction we use this device to demonstrate that the nonequilibrium phonon control mechanism can be used as a local effect to address a single junction. We also analyze the device with respect to a one-dimensional micro-SQUID model that we have developed based on the work of Likharev and Yakobson[15,37] on Dayem bridge Josephson junctions and the numerical analysis of the dc-SQUID by Tesche and Clarke.[14]

II. DEVICE FABRICATION

The micro-SQUIDs with independently controlled junctions were fabricated in a process based on Hutchinson *et al.*[32] in which a micro-SQUID with a single phonon control layer irradiated both junctions was created. The geometry of
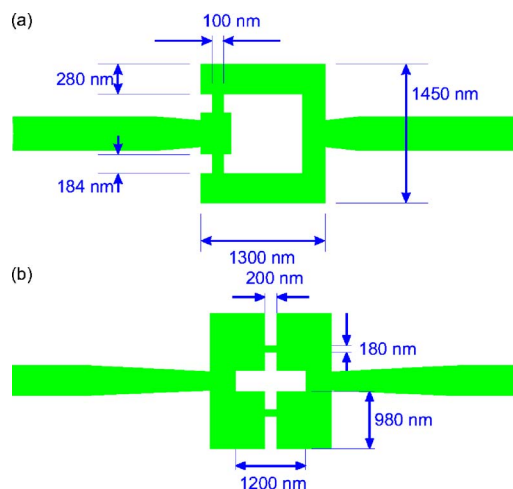

FIG. 1. (Color online) Dimensions of the hot-phonon-controlled micro-SQUIDs (a) with single control and (b) with independent control.

the device had to be extensively modified in order to accommodate the separate control wires for each junction. Hence the device presented in this paper has a more symmetrical geometry, more in common with the nano-SQUID structure[10] than the previous phonon-controlled structure,[32] although many of the dimensions remain comparable as shown in Fig. 1. The fabrication process involved resist patterning using electron-beam (*e*-beam) lithography and thin-film deposition, as well as reactive ion etch and wet etch stages. All lithography stages used *e*-beam lithography to expose a bilayer polymethylmethacrylate (PMMA) resist, consisting of a film of high-molecular-weight resist spun over a film of low-molecular-weight resist, the bilayer chosen to improve the ease of liftoff after metallization stages.

The devices were fabricated on a substrate that consisted of a thick (400 nm) layer of thermally oxidized silicon on a silicon wafer. The superconductor used in these devices was niobium, chosen for its well-known fabrication properties and high critical temperature for an elemental superconductor. The disadvantage of using niobium is its short coherence length, of the order of 38 nm for bulk material,[38] which puts strict limits on the size of junctions that can be used, necessitating the use of electron-beam, rather than optical, lithography to define the structure. A 50-nm film of niobium was deposited onto the cleaned chips via sputtering.

Liftoff processing, in which the lithography is performed in a low-resolution electron beam system with a large current (1 nA) and spot size (250 nm), was utilized to create an etch mask to define the area of niobium in which the micro-SQUID sat and the electrical connections to the dc-SQUID [see Fig. 2(a)]. Next an *e*-beam-patterned area was defined for a thermally evaporated aluminum thin film and was used as a reactive ion etch (RIE) mask to remove the excess niobium. The aforementioned dry etch was performed in an STS RIE 320 system using 40 sccm CF_4 and 4 sccm O_2 at a pressure of 40 mTorr and a power of 300 W. The aluminum mask was then removed in a wet etch stage using a commercial aluminum etchant consisting of a solution of acetic, nitric, and phosphoric acids which was found to efficiently
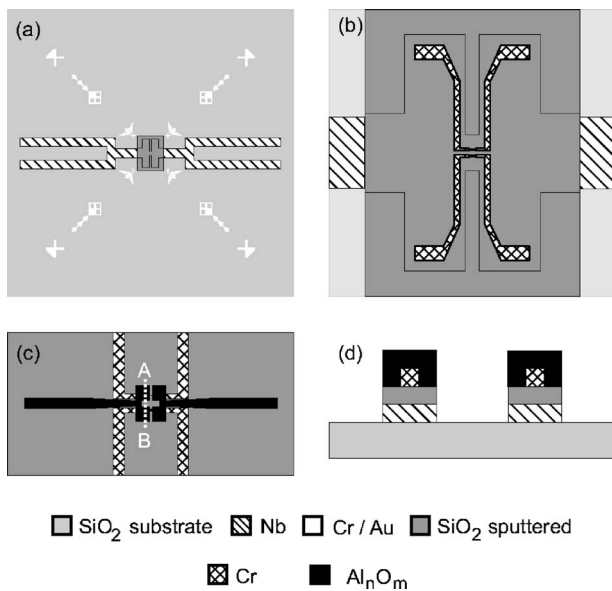
FIG. 2. Schematic diagram of the key fabrication stages of the micro-SQUID with separate phonon control on each junction, as described in the text. (a) shows the region of patterned niobium where the dc-SQUID will be positioned, overlaid in the center with the sputtered SiO_2 film to electrically isolate from the phonon control wires, which are shown in (b). The etch mask for the remainder of the SQUID loop is then deposited (c). Finally (d) shows a cross section along the line defined by $A \rightarrow B$ in (c), after the final reactive ion etch stage. Unlike all the other dimensions in these schematics, the thicknesses, shown in the cross section are not to scale.

remove the aluminum with an undetectable amount of etching of the niobium. The niobium was patterned in this way, using etches, rather than with just a liftoff stage as the quality of the film was found to be better after processing in this way than when deposited through a resist mask.

The development of the device layout was optimized in regards to the fabrication procedure in order to minimize the number of step edges created by the stacked thin films in the design of the device. This consideration is particularly important for the phonon control wires, which had a film thickness, comparable to the niobium thin-film thickness, and therefore step edges of this material were found to regularly cause breaks in the deposited film when it passed from a topographically high region to a low region. Additionally protecting the device from shorting between these electrically isolated layers at these points is also of concern in the device design. The solution to these problems is shown in Fig. 2(a) where "lobes" coming off the central wire were employed in the device design. The thin film used to form the phonon control wires sits entirely over these lobes to prevent such failure.

With the region of niobium that forms the device patterned, 30 nm of amorphous silicon dioxide was then sputter deposited over the central area of the niobium, Fig. 2(a). It is this dielectric layer that isolates the superconductor from the phonon control layers. Thin films of silicon dioxide were often found to have pinholes when sputtered if they were too thin. This thickness of SiO_2 was chosen as it was found to be sufficient to produce a continuous film and hence prevent
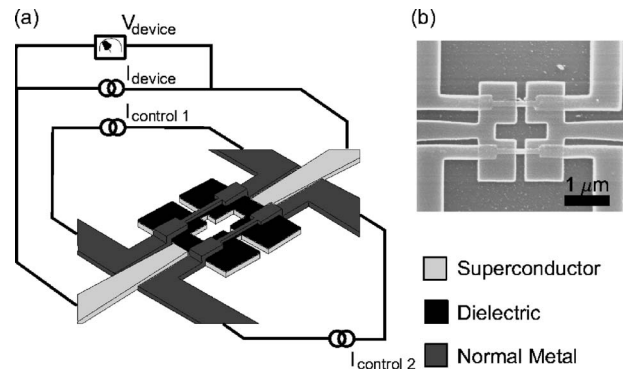

FIG. 3. (a) Shows a schematic of the connections made to the micro-SQUID device, while the inset (b) shows a scanning electron microscope (SEM) image of the device.

shorts from the phonon control wire to the niobium, but thin enough to allow the phonon control mechanism to work. A high-resolution e-beam system was then used to pattern the phonon irradiating wires. In this system there was a user-controlled 1–5pA emission current and a 10–15 nm spot size. The subsequently deposited phonon control wires consisted of 30 nm of thermally evaporated chromium, which was selected as it was found to give a good etch profile.

The micro-SQUID "loop," Fig. 2(c), was defined by a second high-resolution e-beam-patterning process and thin-film deposition and liftoff. In this case, the material chosen to form the loop was aluminum oxide, deposited by thermally evaporating aluminum at a higher pressure (10^{-5} mbar) and at a slower rate (<0.1 nm s^{-1}), than if a nonoxidized aluminum film was required. Aluminum oxide was chosen as it fits the criteria of being a suitable etch mask material and in being resistant to the RIE gasses used to etch the niobium while also being a dielectric, important so that the phonon control wires were not electrically connected to one another. This stage is crucial in determining the final device dimensions; the microbridges due to the positioning of the loop were 200 nm long by 120 nm wide while the area of the loop was approximately 0.6 μm^2. This loop was devised as the combination of several factors. It was found that if the loop was much smaller than this, or indeed slightly larger, it became more difficult to lift off the aluminum oxide in the center of the ring. Additionally a smaller loop results in a larger period of critical-current oscillation in magnetic field, and the loop area had to be optimized in order that several periods of oscillation are seen with the magnetic field used in the experiment.

The electrical connections and bond pads for the micro-SQUID device and the phonon control wires were then patterned, again using the lower-resolution e-beam system. The SQUID itself had four terminals connected so that it could be measured in a four-point arrangement, while the phonon control wires were connected in a two-point configuration, meaning that there were eight connections for each device, and these are shown in schematic form in Fig. 3(a). The material chosen was a thick, 250-nm layer of gold which was deposited on top of a 25-nm-thick layer of chromium for adhesion. The gold also acted as an etch mask protecting the underlying niobium from the final stage of the fabrication

procedure; the etch that transferred the patterns of the various etch masks through to the niobium itself. The final etch used was another reactive ion etch, using the same conditions as described previously, but in this case the timing of the etch was crucial to the successful fabrication of the device. Although the conditions were optimized to produce the most anisotropic etch as possible, there was still a degree of lateral undercutting during the RIE process, and if the duration was too long, the microbridges could be destroyed. However, the etch had to be long enough to remove all the niobium from around the device itself. This stage completed the nanofabrication of the device and left a profile as seen in Fig. 2(d), with the key elements being the niobium film separated from the chromium phonon generating constrictions by the silicon dioxide. A scanning electron micrograph of a completed device is shown in Fig. 3(b).

III. DEVICE CHARACTERIZATION

A. Experimental measurements

The chip containing the fabricated device was mounted into a ceramic header package and secured to the end of a dipstick that could be lowered into a liquid helium Dewar to perform measurements at 4.2 K in a liquid helium bath and allow for electrical connections to be made to the device from outside the Dewar. Electrical connections to the chip used coaxial lines filtered at room temperature. The magnetic field produced for the experiments came from a 4000-turn copper coil mounted around the end of the dipstick, and the current for the coil was supplied from a HP3245A universal source. The micro-SQUID was measured in a four-point configuration using a Keithley 236 source-measure unit (SMU) operating in sweep mode, with separate SMUs controlling the phonon control wires in a two-point arrangement. The measurements were controlled by Labview computer program and consisted of a series of current sweeps, from zero to a bias above the switching point of the device and back down to zero followed by successive steps in the applied magnetic field. In the case of measurements where phonon control was applied, a full magnetic field sweep would be followed by an increment in the phonon control current. The switching points were then extracted from the data and used to generate critical-current oscillation curves in applied magnetic field, the threshold curves.

Measuring the *I-V* curve of the superconducting layer, we show the device was clearly hysteretic as shown in Fig. 4. As the current was ramped from zero, there is a region of zero voltage, the superconducting region, until the critical current is reached at which point the device becomes resistive. The switching current for this device is lower than the micro-SQUID that was investigated earlier without independent phonon control layers[31] which due to the different fabrication methods employed, notably in the deposition of the niobium film, was not unexpected and the critical current remains comparable to other micro-SQUID devices.[2] On the back-sweep the device does not reach the superconducting state until a current much less than the critical current of the device is reached. This is expected and has been investigated for these planar microbridge structures[39] and is the result of
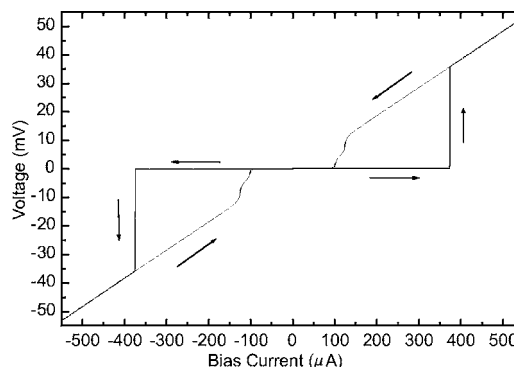

FIG. 4. Current-voltage curve of device. The direction of the current sweep is indicated by the arrows on the diagram.

self-heating hot spots which form when the device switches from the superconducting to normal state. It is this thermal hysteresis that prevents the device from being operated in the voltage mode as phase coherence is lost once the hot spots form and the oscillations in applied magnetic field are not seen. Therefore measurements of the micro-SQUID behavior in a magnetic field are performed as a series of current sweeps to determine the switching current.

Before using the phonon control layers in the device, they were tested for leakage of the control current through to the superconductor that forms the micro-SQUID. These measurements were performed first at room temperature and then at liquid helium temperature to ensure that the dielectric silicon dioxide film had no weak points allowing a conduction path. After passing this test a series of sweeps were made at 4.2 K of the current through the superconductor with fixed values of control current. Figure 5 shows the *I-V* curves for a series of different control currents acting upon just one of the junctions. It can be seen that the curves all have the same normal-state gradient, which is an indication that the temperature of the device is not changing under phonon irradiation.

In Fig. 6(a) we see how the critical current changes upon the application of a control current to a single junction. The maximum current applied to a single control wire for which we still see a superconducting transition is 65 μA; above this value, we were unable to detect a resistanceless state. Once
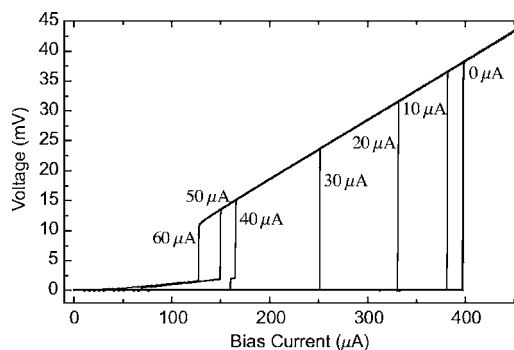

FIG. 5. Current-voltage curve of device under phonon control from only one of the two phonon irradiating wires. In this case for clarity only the forward sweep of the positive branch of the *I-V* graph is shown, for the control currents indicated on the graph.
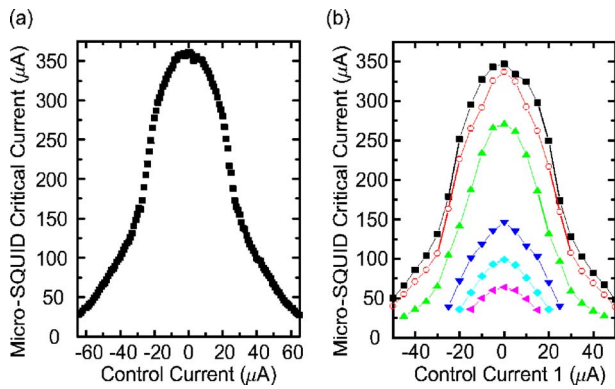
FIG. 6. (Color online) Critical current plotted against control current for (a) the case when a control current is applied to only one junction and (b) when combinations of control currents in each junction are used. In (b) the x axis refers to the control current through wire 1, while the curves from top to bottom correspond to junction-2 control currents of 0, 10, 20, 30, 40, and 50 μA, respectively, the lines joining the points being a guide for the eye.
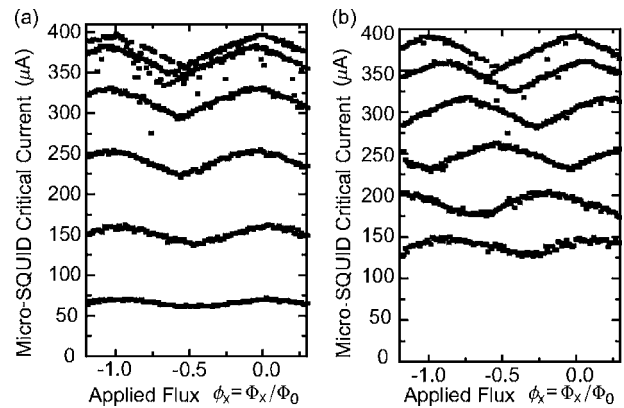

FIG. 7. Critical-current oscillations in applied magnetic field. In (a) an equal control current is applied to each phonon generating wire. In sequence from the top curve to the bottom the applied current is 0 μA, 5 μA, 10 μA, 15 μA, 20 μA, and 25 μA. In (b) the control current is only applied to phonon generation wire 1. Here the curves correspond to an applied current of, again from top to bottom, 5 μA, 10 μA, 15 μA, 20 μA, 25 μA, and 30 μA.

the phonon control had been tested for one junction, it was then checked for both junctions simultaneously, and in Fig. 6(b) we show the effect on the critical current for a number of combinations of the control current. In this device clearly the control current works in both of the junctions, where it was observed that the same current applied to each of the junctions had a similar effect on the critical current of the respective junctions.

Measurements on the device were subsequently performed to determine the behavior of the device in an applied magnetic field. A time delay was included within the measurement software after the increment of the magnetic field in order to ensure that the coil circuit has settled before the current sweep was performed. The device was indeed found to have the critical-current oscillations expected of a dc-SQUID, while no voltage oscillations could be detected with a bias greater than the critical current of the device due to the thermal effect described above. The micro-SQUID device was found to exhibit periodic oscillations of the critical current in the applied flux, as seen in Fig. 7. The left-hand panel, Fig. 7(a), shows a series of curves that correspond to equal currents being applied to each of the two phonon control wires in the device. The threshold curve for zero applied control current shows the triangular oscillations with a relatively small modulation depth that are characteristic of micro-SQUID devices, particularly in niobium as there is a nonsinusoidal current phase relationship that exists for a Dayem bridge Josephson junction in the "long" limit.[15] It can be seen that increasing the control current has the effect of reducing the critical current of the device overall as well as causing the oscillations to become less triangular.

In the critical-current oscillation data it was observed that magnetic hysteresis for small values of control current was present. This is a common effect that occurs due to alternative flux states at particular values of applied magnetic field that correspond to either clockwise or anticlockwise circulating currents in the loop. In Fig. 7(b) we plot results where the control current is applied to only one of the phonon-generating constrictions; that is, the current through the other

is set as zero. Here we observe that as the device becomes asymmetric the maxima of the oscillations move with respect to one another. We show later that this is consistent with our one-dimensional model for the behavior of asymmetric micro-SQUIDs in which we see a translation of the curve along the flux axis in one direction or the other dependent upon which junction is irradiated. The other notable effect, seen most visibly in the curves with the largest applied control current, is that the shape of the oscillation is no longer symmetric about the maximum, again something consistent with our model. Our results therefore show that we are able to address each junction separately in order to modify the threshold characteristics of the device post-fabrication. In this way we can distort the curves to make them asymmetric, shift the maxima and minima of the curves, eliminate magnetic hysteresis, and modify the shape from a triangular to a more rounded oscillation.

B. Hot-phonon control mechanism

The operating mechanism for the critical current control exhibited in the device is a result of the nature of the thermal decoupling between the phonons and electrons in the hot-phonon injection material, which occurs at low temperatures.[40–42] Due to this decoupling, the application of an electric field across the metallic hot-phonon injection layer causes the electron system to be heated to a temperature T_e above the temperature of the phonon bath. Since the electrons are heated above the lattice equilibrium temperature, the inelastic relaxation process of these hot electrons is more likely to produce "hot phonons" that change the equilibrium distribution of the phonons at the temperature of the helium bath.

From the work of Nabity and Wybourne[43] on the phonon escape from electrically heated metal films on silicon dioxide, it is found that the transport at low temperatures consists of ballistic transport of the phonons out of the metallic film

with strong scattering at the interface between the materials. After generation, the low-frequency phonons escape from the film with a time scale that is faster than the time scale for the phonon to be scattered from an electron. The analysis shows that there is a phonon frequency dependence in the phonon escape time, which means that the injected phonon distribution is not a thermal distribution, and for much higher frequencies the phonon escape is longer than that predicted by an acoustic mismatch model[44,45] and traps these in the metallic film. This is thought to be the result of phonon scattering in the silicon dioxide, which is particularly relevant in the case of the hot-phonon-controlled device since the material is amorphous. Here we note that the high-frequency phonons that are trapped in the hot-phonon injection film are of much larger energy than 2Δ, where Δ is the superconducting energy gap that corresponds to the bound energy of the Cooper pairs in the superconducting layer.

Once the nonthermal population of hot phonons has been injected into the Dayem bridge Josephson junction, they are absorbed by the Cooper pairs provided they are of energy 2Δ or greater. This is the smallest amount of energy that must be supplied to the Cooper pair to depair it and create two quasiparticle excitations from the superconducting condensate. Since the superconducting state is an ensemble state consisting of bound electron pairs, which reduce the overall energy of the system, then by increasing the number of quasiparticle excitations in the superconductor through hot-phonon absorption, the superconducting state has a reduction in the superconducting energy gap Δ and hence a reduction in its critical current. The phonons that have less than 2Δ energy can only interact with other quasiparticle excitations or other elastic scattering mechanisms due to defects or impurities. In general, these will exit the superconductor to the substrate.

A characteristic of a microbridge junction is that the superconducting order parameter is suppressed in the region of the Dayem bridge constriction. This region, by the design of the hot-phonon-controlled Dayem bridge Josephson junction, is irradiated with the greatest flux of hot phonons so that the superconducting order parameter in this constriction is further suppressed and, therefore, lowers the critical current of the junction. Increasing the phonon irradiation in this region, by increasing the voltage across the phonon injection layer, results in the coupling between the superconducting wave function in the banks of the Dayem bridge Josephson junction being destroyed by the reduction of superconducting order parameter to zero in this region, hence fully suppressing the observed Josephson effect in the device. This is the full mechanism by which the critical-current control of the Dayem bridge Josephson junction is achieved. To observe this effect it is important that in the design of the device the voltages applied to the hot-phonon injection layer, to control the device, should be small enough so that Joule heating of the device above its critical temperature does not occur.

Using a finite-element method we now demonstrate that the resistive heating due to the control current in the phonon-injection wire is insufficient to account for the change in critical current that we see in our device. This model has been developed in order to give an overestimate of the temperature increase in order to determine an upper limit. Therefore we discount many well-known cooling mechanisms and
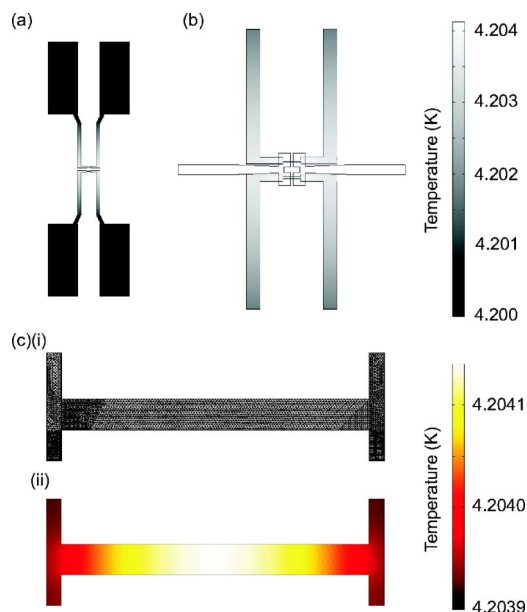

FIG. 8. (Color online) Plot of the results of the finite-element analysis of the heating effects due to the control current, for a control current of 20 μA. (a) Full area heating model showing bond pads. (b) Close-up of micro-SQUID hot-phonon injection constrictions. The micro-SQUID pattern is shown by the superimposed dotted line. (c) Heat generated in the constrictions, with (i) showing the finite-element mesh and (ii) the temperature distribution in the bridge.

include only thermal conduction in the control layer and heat transfer to the helium bath as modes of heat loss.

We use a two-dimensional model of the phonon control region and use the resistive heating module in the finite-element software, in conjunction with the heat transfer module to get a temperature profile of the device, as shown in Fig. 8. The model solves the two-dimensional heat flow equation to determine the temperature T at any point:

$$-K\nabla^2 T + \frac{\alpha}{d}(T - T_{He}) = \rho J^2, \quad (1)$$

in which K is the thermal conductivity at helium bath temperature T_{He}, α the heat transfer coefficient from the film to the helium bath, ρ the resistivity of the film, J the current density, and d the film thickness. The boundary conditions are set so that the temperature of the phonon control wire under the thick gold contact pads is the bath temperature, 4.2 K, a suitable approximation as the cooling area is much larger. The value of thermal conductivity used in the model, is an experimentally determined value of 160 W/m K.[46] In the calculation resistivity of chromium of 0.5×10^{-8} Ω m is used which is the value at 78.2 K.[47] The value at 4.2 K is expected to be lower than this, so again this will contribute to the overestimate of the temperature increase.

A plot of the model results is shown in Fig. 8. For a control current of 20 μA applied to just one of the phonon control wires, a decrease in the critical current of the device is seen from 397 μA to 288 μA. From measurements of the temperature dependence of the critical current we would ex-

pect this reduction to be accompanied by an increase in temperature of at least 0.25 K. The model shows that the largest temperature rise that we could expect for this control current would be only 0.004 K, less than 2% of the temperature rise needed. Similarly, the control current that was found to completely suppress the superconductivity was 65 μA, while the model shows that this would only produce a temperature rise of 0.043 K and in reality a temperature increase of at least 1.4 K would have been required to destroy the superconducting state.

This modeling demonstrates that the equilibrium temperature rise due to Joule heating is insufficient to account for the extent of suppression of the critical current that is seen for an applied control current. This suggests that the mechanism responsible is a result of a nonequilibrium state as described above, with the "hot phonons" generated in the injection layer suppressing the order parameter through the creation of quasiparticle excitations as Cooper pairs are destroyed.

IV. NUMERICAL ANALYSIS OF AN EXPERIMENT USING A ONE-DIMENSIONAL micro-SQUID MODEL

We now turn our attention to formulating a model to describe the behavior of our device under phonon irradiation. We begin by examining, through a one-dimensional solution of the Ginzburg-Landau equation, the supercurrent-phase relationship in a Dayem bridge-type junction. We then take this result and formulate a model for the micro-SQUID device from which we can calculate the critical-current threshold curves in applied magnetic field.

A. Dayem bridge Josephson-junction supercurrent-phase relationship

The definition of a superconducting weak link, which is given by Likharev,[15] states the three properties that a Josephson junction must have: (i) The Josephson junction supercurrent-phase relationship $I_0(\varphi)$ is 2π periodic so that $I_0(\varphi + 2\pi) = I_0(\varphi)$. (ii) The supercurrent in the Josephson junction is zero when the phase difference φ across the junction is an $n\pi$ for any integer n. (iii) The Josephson-junction supercurrent-phase relationship is symmetric so that $I_0(-\varphi) = -I_0(\varphi)$.

The Dayem microbridge Josephson junction[13] that consists of a constriction in a superconducting thin film, which is itself superconducting but with a reduced critical temperature T'_C, adheres to these three principles. Only when the length of the bridge is comparable or much less than the coherence length of the superconducting thin film can one observe the classic Josephson effect $I_0 = I_C \sin\varphi$; the simple derivation of this is found in many introductory texts.[48–51]

Now for microbridges that have a length L, which is comparable or longer than the superconducting thin-film coherence length ξ, we briefly demonstrate the analysis of Likharev and Yakobson.[15,37,52] Here, when we consider the reduced Ginzburg-Landau differential equation—that is, in the absence of fields and writing $f(x) = a(x)\exp[i\varphi(x)]$ and $f(x) = \varphi(x)/\varphi_\infty$—we can derive the equation
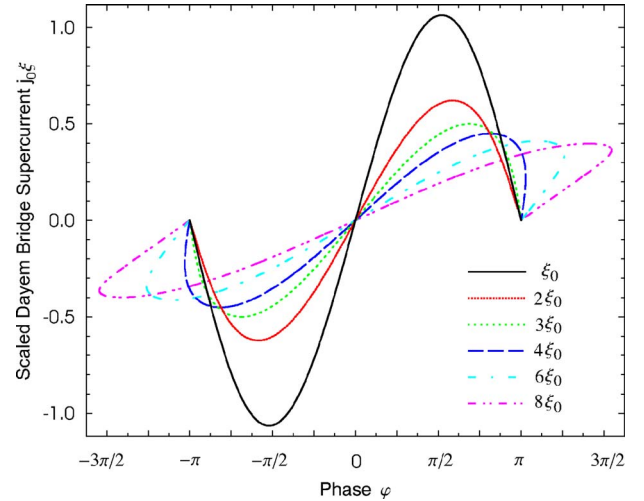

FIG. 9. (Color online) Supercurrent-phase relation for Dayem bridge junctions of varying length. The bridge lengths are shown in the legend with respect to the coherence length ξ.

$$\xi\frac{d}{dx}a(x) = \sqrt{k - a(x)^2 + \frac{a(x)^4}{2} - \frac{j_0^2}{a(x)^2}},\qquad(2)$$

where the scaled current density is

$$j_0 = \frac{J_0 m}{\hbar e \psi_\infty^2} = a(x)^2\frac{d}{dx}\varphi(x)\qquad(3)$$

and the characteristics of the solution $a(x)$ require that at the microbridge banks be the bulk superconducting wave function ψ_∞ so that $a(0) = a(L) = 1$. Also, in the region of the microbridge, the amplitude of the wave function is weakened, meaning that $a(x) < 1$, and has its minimum a_0 at the center of the bridge. This yields $a(L/2) = a_0$ and, therefore,

$$k = a_0^2 - \frac{a_0^4}{2} + \frac{j_0^2}{a_0^2}.\qquad(4)$$

From Eq. (2) the supercurrent-phase relationship for a Dayem bridge of arbitrary length can be constructed so that the bridge length L (or l in units of ξ) is

$$l = \frac{L}{\xi} = 2\int_{a_0}^1 \frac{da}{\sqrt{k - a(x)^2 + \frac{a(x)^4}{2} - \frac{j_0^2}{a(x)^2}}}\qquad(5)$$

and the phase difference across the Dayem bridge Josephson junction is

$$\varphi = 2j_0\xi\int_{a_0}^1 \frac{da}{a^2\sqrt{k - a(x)^2 + \frac{a(x)^4}{2} - \frac{j_0^2}{a(x)^2}}}.\qquad(6)$$

By numerically integrating Eqs. (5) and (6) in conjunction with a two-dimensional root-finding algorithm, we find j_0 and a_0 for a given bridge length l and phase difference φ.

In Fig. 9 we show the result of performing this numerical calculation for such a variety of Dayem bridge lengths. For a bridge of length ξ we find that the supercurrent-phase rela-
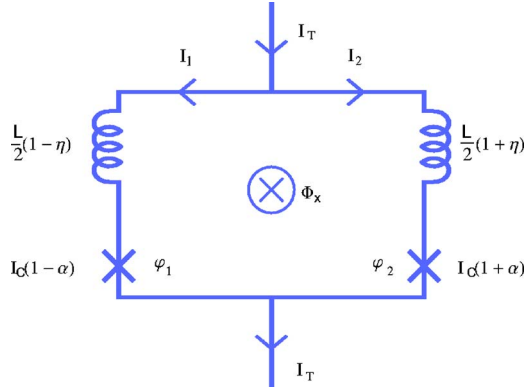
FIG. 10. (Color online) Circuit diagram for a dc-SQUID.

tion is approximately the classical Josephson relation. This means we typically classify the Dayem bridge Josephson junctions so that when $L \leq \xi$ it possesses the classical Josephson effect. As the microbridge becomes longer, the supercurrent-phase relationship become less sinusoidal. When the length of the microbridge is 3ξ it has become double valued. Here we note that although the shape of the supercurrent-phase relationship moves markedly away from the sinusoidal shape, it still satisfies the three principles defined for Josephson-junction weak-link behavior. As the length is increased up to 8ξ we see that the maximum of the supercurrent-phase relationship decreases to a constant value. This constant value is the depairing critical-current density

$$J_C = \frac{2}{3\sqrt{3}} \frac{\hbar e \psi_\infty^2}{m\xi} \quad (7)$$

of an infinitely long superconducting wire.[48]

B. One-dimensional micro-SQUID model

Having reviewed the method for obtaining the current-phase relationship for the Dayem bridge Josephson junctions in the preceding section, we can now use this result in conjunction with the analysis provided by Tesche and Clarke[14] wherein we substitute our calculated current-phase relationship for the ideal, sinusoidal relationship in order to calculate the characteristics of a micro-SQUID device.

To explain this analysis we consider the superconducting loop containing two Josephson junctions shown in Fig. 10. The device is biased by a total current $I_T = I_1 + I_2$ where I_1 and I_2 are the currents flowing in the two arms of the dc-SQUID. These currents, given in their most general form appropriate for a Dayem bridge Josephson junction, are given by

$$I_n = I_{Cn} F_{ln}(\varphi_n), \quad (8)$$

where I_{Cn} is the maximum critical current obtained by the Josephson junction, labeled by the index $n \in \{1, 2\}$, for all φ_n, where φ_n is the phase difference across junction n and the function $F_{ln}(\varphi_n)$ denotes the supercurrent-phase relationship for a bridge of length L so that $l = L/\xi$.

Each arm of the dc-SQUID is represented by an arm inductance L_1 and L_2, where $L = L_1 + L_2$ and L is the total inductance of the loop. On each arm is a Josephson junction

with critical currents I_{C1} and I_{C2}. To account for an asymmetric double-junction configuration we introduce the parameters η and α for the arm inductance and Josephson-junction critical current so that we can write

$$L_1 = \frac{L}{2}(1 - \eta) \quad \text{and} \quad L_2 = \frac{L}{2}(1 + \eta) \quad (9)$$

for the arm inductance and similarly for the critical current:

$$I_{C1} = I_C(1 - \alpha) \quad \text{and} \quad I_{C2} = I_C(1 + \alpha), \quad (10)$$

where I_C is the average critical current of the two junctions. The loop is biased by an external flux Φ_x that contributes to the total flux Φ enclosed by the dc-SQUID loop. By an analysis of the circuit we can write the effective flux Φ through the loop as

$$\Phi = \Phi_x + \frac{LI_2}{2}(1 + \eta) - \frac{LI_1}{2}(1 - \eta) = \Phi_x + LI_S + \frac{\eta}{2}LI_T, \quad (11)$$

where the circulating current in the dc-SQUID loop is represented by $I_S = (I_2 - I_1)/2$. Finally, since the phase around the loop is single valued, then in terms of the gauge invariant phase differences φ_1 and φ_2 across the two Josephson junctions we have

$$\varphi_1 - \varphi_2 = 2n\pi + 2\pi \frac{\Phi}{\Phi_0}. \quad (12)$$

From these relations we can derive a set of three coupled equations that govern the critical current properties of the dc-SQUID relative to an applied flux. From the relations $I_T = I_1 + I_2$, $I_S = (I_2 - I_1)/2$ and the combination of Eqs. (11) and (12), we respectively find the following set of three coupled equations:

$$i_S = \frac{(1 + \alpha)F_{l2}(\varphi_2) - (1 - \alpha)F_{l1}(\varphi_1)}{2}, \quad (13)$$

$$i_T = (1 - \alpha)F_{l1}(\varphi_1) + (1 + \alpha)F_{l2}(\varphi_2), \quad (14)$$

and

$$\varphi_2 = \varphi_1 - 2\pi\phi_x - \beta i_S - \frac{\beta \eta i_T}{2}, \quad (15)$$

where

$$\beta = 2\pi \frac{LI_C}{\Phi_0}, \quad (16)$$

$\phi_x = \Phi_x/\Phi_0$, $i_T = I_T/I_C$, and $i_S = I_S/I_C$. From Eqs. (13)–(15) we find the critical current of the dc-SQUID relative to an applied flux by finding the maximum current i_T for a chosen ϕ_x. To do this, we substitute Eqs. (13) and (14) into Eq. (15), and we express φ_2 as a function of φ_1 and i_T. Doing so we have

$$\varphi_2 = \varphi_1 - 2\pi\phi_x - \frac{\beta i_T(1 + \eta)}{2} + \beta(1 - \alpha)F_{l1}(\varphi_1), \quad (17)$$
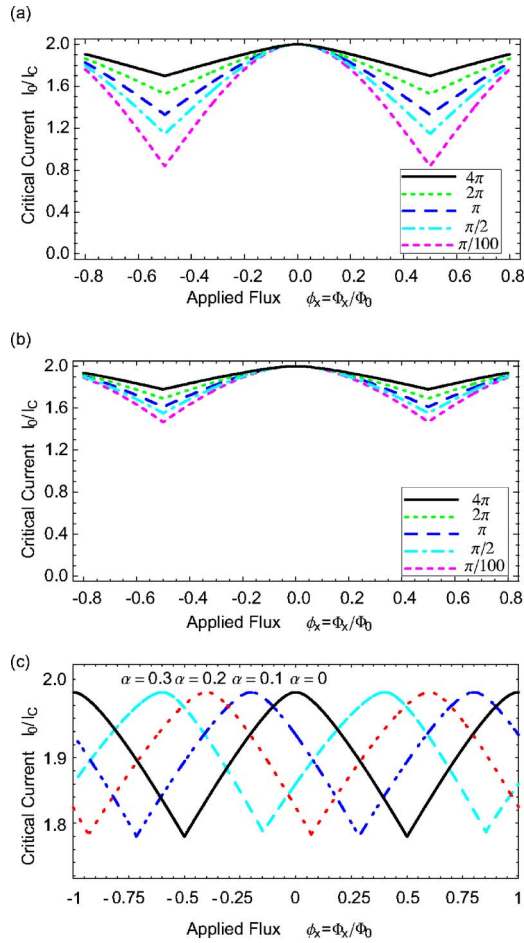
which allows us to define a function G of i_T and φ_1:

FIG. 11. (Color online) Numerical plots of micro-SQUID critical-current oscillations curves. The curves in (a) and (b) correspond to β values of 4π, 2π, π, $\pi/2$, and $\pi/100$ (in order from top to bottom and represented by the line styles in the legend), which contain Josephson-junction Dayem bridges of length (a) $4\xi_0$ and (b) $8\xi_0$, while (c) shows the effect of changing the α parameter for a fixed bridge length of $8\xi_0$ and β value of 4π.

$$G(i_T, \varphi_1) = i_T - F_{l1}(\varphi_1) - F_{l2}(\varphi_2). \qquad (18)$$

As was the case for the dc-SQUID, the critical current of the micro-SQUID for a given applied flux ϕ_x occurs for the greatest i_T that satisfies $G(i_T, \varphi_1)=0$ for some φ_1 when

$$\frac{\partial G(i_T, \varphi_1)}{\partial \varphi_1} = -\frac{\partial}{\partial \varphi_1} F_{l1}(\varphi_1) - \left(1 + \beta \frac{\partial}{\partial \varphi_1} F_{l1}(\varphi_1)\right) \frac{\partial}{\partial \varphi_1} F_{l2}(\varphi_2)$$

$$= 0. \qquad (19)$$

We find simultaneous zeros of Eqs. (18) and (19) using a numerical root-finding program in the two-dimensional (i_T, φ_1) space for specified functions F_{ln}, determined by the bridge length l_n of each of the junctions for a specified ϕ_x and β parameter.

In Figs. 11(a) and 11(b) we show the results of our calculations for micro-SQUIDs in which we assume identical Dayem bridge junctions with a length of 4 and 8 coherence lengths ξ. Each of these plots show the critical current oscillations for the β parameter with values of 4π, 2π, π, $\pi/2$,

and $\pi/100$. In these plots we show that by using longer Dayem bridge Josephson junctions in a micro-SQUID, the critical current modulation depth is decreased. In terms of using these devices for sensitive magnetometers, a reduced critical-current modulation is an undesirable characteristic as it reduces the device's discriminating ability relative to intrinsic noise. This means that when choosing the thin-film material to construct the micro-SQUID a choice based on the critical temperature and characteristic coherence length must be considered. For instance, to operate below temperatures of about 9 K, we would ideally use niobium since it has well-known fabrication properties. However, as mentioned in Sec. II niobium's drawback is its short coherence length which puts a considerable fabrication constraint on the Dayem bridge dimensions.

From Fig. 11 we show that for a value of $\beta=4\pi$ and longer Dayem bridge lengths the shape of the critical-current oscillation departs from the "sinusoidal" shape and becomes more "triangular." This characteristic is also shown by Hasselbach *et al.*[53] whose analysis goes another step further than our one-dimensional approach of the Dayem bridge junctions by using the Ginzburg-Landau theory to model a two-dimensional micro-SQUID structure comprising of the two Dayem bridge junctions and the adjoining loop. Although our results are in qualitative agreement with this two-dimensional analysis, their analysis shows that unlike the assumption made in our model, the suppression of the superconducting order parameter ψ by the reduced dimensions of the Dayem bridge Josephson junctions extends into the micro-SQUID loop and is not just confined to the junction. This characteristic of micro-SQUIDs, with Dayem bridge lengths larger than the coherence length of the thin film, is particularly relevant to devices made from niobium. This is a result of the relatively short coherence length observed in this thin-film material, since it is close to the smallest feature size that can be routinely achieved using high-resolution electron-beam lithography, which is around 20–30 nm.

The reduction of the critical-current modulation ΔI_0 for various Dayem bridge lengths is shown in Fig. 12. Here the plot of the critical-current modulation versus the β parameter for Dayem bridges of length 2, 4, 6, and 8 coherence lengths ξ is shown, which shows the loss of modulation for the longer Dayem bridge junctions. In Fig. 12(a) the critical-current modulation depth ΔI_0 is plotted as a function of the inductance, and shows that the micro-SQUIDs do not achieve a value of 1 as the inductance of the loop approaches zero. Figure 12(b) shows the change in the modulation depth as a function of the critical current I_C since the modulation depth is proportional to the critical current of the device. Here, the modulation depth approaches the limit Φ_0/L for large I_C. In general, due to the bridge length characteristic of the micro-SQUID, their application is not driven by the need for sensitive magnetic measurements but rather the need for local magnetic measurements that can discriminate from nonlocal background fluctuations.

Having used the model to demonstrate the effect of changing the coherence length of both junctions simultaneously, we can now consider the effect that a change of the α parameter that represents the asymmetry of the junction critical currents has on the critical current oscillations. Figure
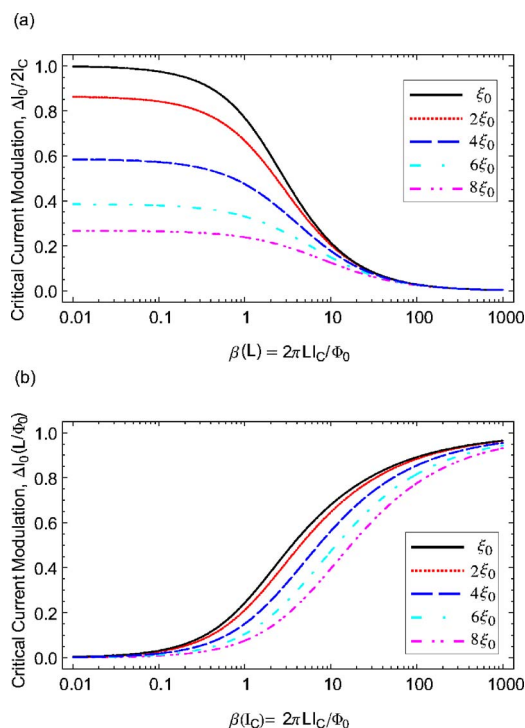
(a)

(b)

FIG. 12. (Color online) Critical-current modulation for a micro-SQUID as a function of (a) inductance and constant critical current and (b) critical current and constant inductance, for bridge lengths of $8\xi_0$, $6\xi_0$, $4\xi_0$, $2\xi_0$, and ξ_0 as indicated by the inset legends.

11(c) shows the effect of introducing an asymmetry into the critical currents of the junctions; we show that by increasing the value of α we get a reduction in the modulation depth of the oscillations and a distortion of the curve, which is most notable in the shift of the maxima and minima along the flux axis. The graphs shown in Fig. 11(c) demonstrate the case when the critical current of the first junction is reduced with respect to the second junction. If the situation were reversed, we would expect an equal shift in the opposite direction along the flux axis. It can also be seen that as the α parameter increases, the distortion of the oscillation means that the magnitude of gradient of one side of the curve increases with respect to the other side.

C. Analysis of experimental critical-current threshold curves

Having developed our one-dimensional micro-SQUID model previously, we are now able to analyze the results of Hutchinson *et al.*[31] for a micro-SQUID in which a single phonon-generating layer controlled both junctions simultaneously in the context of our micro-SQUID model, as well as the data presented in this paper. In terms of the first device, we find that the critical-current control mechanism is effectively shortening the Josephson junctions since the coherence length in the film is lengthening. We demonstrate this by using the procedure of generating the Dayem bridge supercurrent-phase relationship for a chosen effective length L_{eff} such as those shown in Fig. 9 and then applying the dc-SQUID numerical equations given by Eqs. (13)–(15) to produce the plots of the critical current modulation versus a
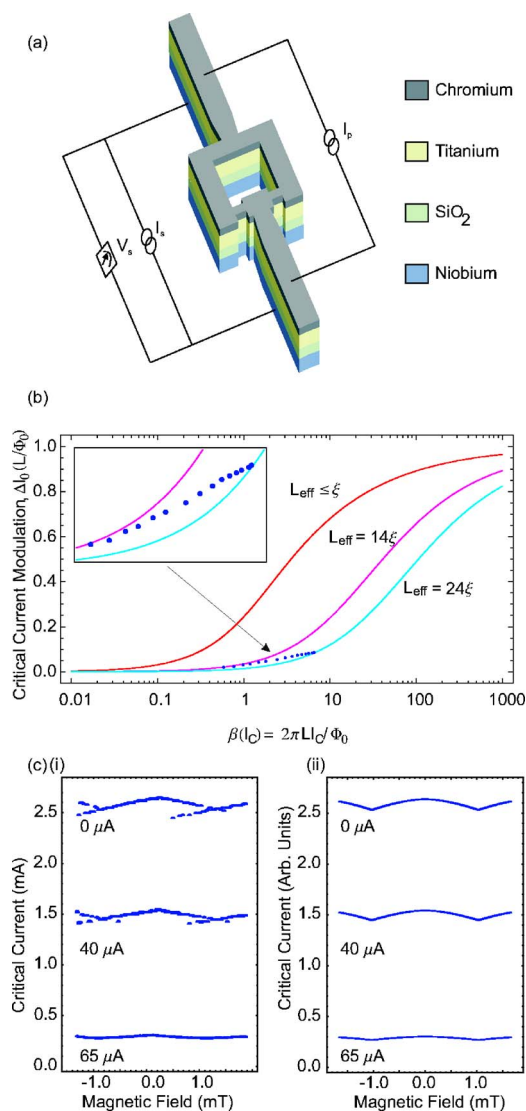

(a)

(b)

(c)(i)   (ii)

FIG. 13. (Color online) (a) Schematic of the single-control-layer device. I_p refers to the phonon control current, while I_s and V_s refer to the current source and voltage measurement of the micro-SQUID. (b) Experimental critical-current modulation data shown versus the critical-current modulation curves for bridges of effective length $L_{eff}=14\xi$ and 24ξ for this device. These curves have been predicted using the one-dimensional micro-SQUID model discussed in the text. The top curve corresponds to the critical-current modulation curve for the dc-SQUID with the classical Josephson effect. (c) (i) Experimental results from the nonindependent junction device and (ii) the fit of our one-dimensional model to the data. The labels on the curves correspond to the phonon control current.

change in the critical-current given in Eq. (12).

In Fig. 13 we show the computed curves for a Dayem bridge of effective length 14ξ and 24ξ and they are plotted with the experimental data. The data show that the effective length L_{eff}, the region where the superconducting order parameter is suppressed in the device, is initially 24 coherence lengths long. The theoretical work of Hasselbach *et al.*[53] contained a two-dimensional model that showed for Dayem bridge's with a geometrical length of 184 nm at 4.3 K corresponds to a geometrical bridge length of 9.4ξ long with

further suppression of the order parameter outside this region. He therefore showed that the superconducting order parameter in the micro-SQUID was not confined to the geometry of the Dayem bridge constriction, which agrees with our result of L_{eff} being of the order of 24ξ. As the control current I_h is applied to the controlled micro-SQUID, then from the data shown in Fig. 13(b), the coherence length ξ gets longer as the effective length of the bridge becomes shorter relative to ξ. Using these values it can be seen in Fig. 13(c) that we get a good fit from our model for the experimental data.

When the control current is 65 μA, the critical-current maximum of the micro-SQUID is 297 μA with a modulation depth of 31 μA. This was the highest control current applied in the experiment where a critical-current oscillation was detected in the micro-SQUID. In Fig. 13 we show that when the control current is 65 μA the effective length of the Dayem bridges has shortened to 14ξ. This shows that by irradiation with hot phonons, the coherence length in the hot-phonon-controlled micro-SQUID device lengthens. Such an observation is consistent with Ginzburg-Landau theory which gives

$$\xi(T) = \frac{\hbar}{\sqrt{4m|\alpha(T)|}} \propto \frac{1}{\sqrt{1 - T/T_C}} \qquad (20)$$

and shows that the coherence length of the superconducting material lengthens with temperature and therefore lengthens as the binding between the electrons in the Cooper pairs weakens (see Refs. 48, 49, and 54). However, although the lengthening of the coherence is expected with hot-phonon irradiation, this does not mean that the process should be viewed as a process to simply manipulate the temperature of the device but rather a more complicated mechanism in which the superconducting order parameter is suppressed in a nonequilibrium process.

We know from the fit of our model to the single-control-layer device that irradiation with hot phonons increases the coherence length in the junction while reducing the critical current, and we have seen that an asymmetry in the junction critical currents distorts the threshold curves. From the observations and analysis of this device we see that in order to fit the model to our asymmetrically controlled micro-SQUID device we must take into account both the change in critical current and coherence length that occurs upon the application of the hot-phonon irradiation. The reduction in critical current of one junction compared to the other is manifested in the α parameter while the effective length of each junction determines the function $F_{ln}(\varphi_n)$ which can be chosen separately for each junction in the model. Additionally the value of the β parameter will change as the critical current of the device as a whole is adjusted.

The first stage in applying the model to the experimental data is to fit an effective bridge length to the data in which no phonon control is applied to either of the junctions and the device is assumed to be symmetric. This then gives a starting point for fitting to subsequent curves as only one of the junctions is irradiated. The α and β values are calculated from the change in the critical current of the device under varying
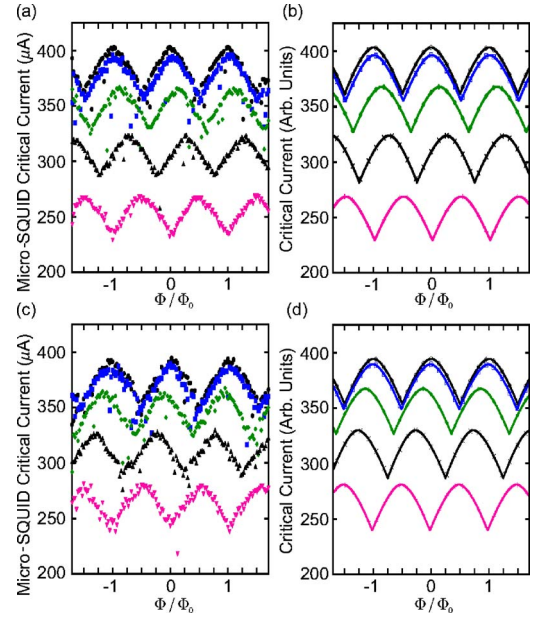

FIG. 14. (Color online) Plot of modeled data and experimental results for a micro-SQUID device in which each junction was controlled separately. (a) shows the experimental results with control currents applied to junction 1 only, with (b) showing the modeled fit to the data. (c) is the case when control currents were applied to bridge 2 only and this situation is modeled in (d). In all cases the curves correspond from top to bottom to applied control currents of 0, 5, 10, 15, and 20 μA, respectively.

phonon control currents. The value of the inductance of the device, 2.1π pH, which features in the β parameter, is calculated from a computer simulation of the device using the 3D-MLSI program designed for superconducting devices.[55] The effective bridge length of the irradiated junction is then varied as a fitting parameter. Note that we assume no asymmetry in the inductance—that is a value of η of 0.

Experimental results for the independent junction device are shown in Fig. 14 along with the fit of the one-dimensional model. It can be seen that our model gives a very good fit to the experimental data. Magnetic hysteresis is not shown in the modeled results as in the modeling procedure the maximum switching current is chosen for a particular value of applied flux. The parameters used to fit to the data are shown in Table I. Clearly the effective length is reducing as the bridge is irradiated, as we expected following the analysis of the symmetrically controlled micro-SQUID

TABLE I. The values of the parameters used in the model to generate the curves of Fig. 14. Here L_n refers to the ratio of the effective length of bridge n to the coherence length ξ in the bridge.

Control current (μA)	β/π	α	L_1	L_2
0	1.31	0	13	13
5	1.29	0.05	13	13
10	1.20	0.13	12	13
15	1.05	0.28	10	12.5
20	0.87	0.54	8	12.5

device. The bridge length to coherence length ratio at 4.2 K with no phonon control is different from that device due to both the different device geometry and the use of a different set of superconducting films in the fabrication of each device. For the control currents of 15 μA and 20 μA the effective length of the nonirradiated bridge is reduced slightly to 12.5ξ. Hence, although the control couples into the junction that it addresses to a far greater extent than the opposite junction, there is a small effect on the other link. This may be due to the fact that the constrictions in the phonon generating wire are longer than the Dayem bridges of the micro-SQUID, so that although the hot-phonon generation is largely over the microbridge, there is some effect on the superconductor in the loop banks. However, the difference in the magnitude of the effects suggests that this mechanism is consistent with the independent control of the two Josephson junctions.

The movement of the maxima along the flux axis, as predicted by the simple model for changing α is seen clearly as the phonon control current is increased. Indeed, for a control current of ± 20 μA there is now a minimum of the threshold curve where for no control current we see a maximum. It can also be seen that application of the control current to bridge 2 results in similar curves to those obtained with the control applied to bridge 1, only reflected in the $\phi/\phi_0 = 0$ axis. This is what we would expect from the theory as when we start with a symmetric device the two junctions are equivalent and a change due to one junction would be equivalent to an equal but opposite change in the other. The fit of our data to our model validates the approximation that we employed in using a one-dimensional solution of the Ginzburg-Landau equation to our device. Indeed the symmetry of the geometry of the independently controlled micro-SQUID, when compared with the micro-SQUID with a single control layer, means that the one-dimensional model is perhaps more relevant to our new device as any suppression of the superconducting order parameter outside of the bridge region will be symmetric as our loop banks are the same on either side of the bridge.

V. CONCLUSIONS

In this paper we have reported the successful fabrication of micro-SQUID devices which can be made asymmetric post-fabrication by suppressing the critical current of either of the junctions individually by irradiation with hot phonons

generated in a normal-metal chromium constriction electrically isolated from, but in close proximity to the microbridge junctions. We have shown that this method of control can be used with two Josephson elements in the same device to control each independently of the other in this proof-of-principle device. Additionally we have analyzed both this device and a more simple micro-SQUID in which both junctions were controlled by a single-phonon-generating layer in terms of a one-dimensional model tailored for the nonsinusoidal current phase relationships exhibited by micro-SQUIDs.

According to our model, we have shown that the short coherence length ξ in the niobium thin film relative to the Dayem bridge's effective length meant that the hot-phonon-controlled micro-SQUID consisted of two "long" Josephson junctions for both types of devices. Therefore, in both cases the supercurrent-phase relationship for these Josephson junctions was not the classical Josephson effect, but one altered due to the depairing effect of the current flowing in the bridge. This supercurrent-phase relationship, in combination with a large β parameter, meant that the critical current oscillations observed had a triangular shape. The application of the control current was shown to have the effect of lowering the critical current of the device as well as increasing the coherence length of the niobium film as the hot phonons break Cooper pairs in the device. We were therefore able to demonstrate the ability to adjust the asymmetry of the device which is clearly shown in shifts of the critical current oscillations along the flux axis.

This hot-phonon-controlled device demonstrated that this type of critical-current control for Dayem bridge Josephson junctions is suitable for use in the micro-SQUID device configuration, since it does not destroy the phase coherence across the Dayem bridge (and thus preserving the Josephson effect), while reducing the critical current. That is, it allows for the manipulation of the Josephson effect, which results in control of the critical current in the device. Further to this we have shown that by fabricating separate control wires for each Dayem bridge, the critical current of each Josephson junction can be controlled locally and demonstrated how this can then be used to adjust the asymmetry of the device.

*Electronic address: gp278@cam.ac.uk

[1] R. L. Fagaly, Rev. Sci. Instrum. **77**, 101101 (2006).

[2] K. Hasselbach, C. Veauvy, and D. Mailly, Physica C **332**, 140 (2000).

[3] C. Chapelier, M. E. Khatib, P. Perrier, A. Benoit, and D. Mailly, in *Superconducting Devices and Their Applications: Proceedings of the 4th International Conference SQUID '91*, edited by H. Koch and H. Lübbig (Springer-Verlag, Berlin, 1992), pp. 286–291.

[4] C. Thirion, W. Wernsdorfer, and D. Mailly, Nat. Mater. **2**, 524

(2003).

[5] W. Wernsdorfer, E. B. Orozco, K. Hasselbach, A. Benoit, B. Barbara, N. Demoncy, A. Loiseau, H. Pascard, and D. Mailly, Phys. Rev. Lett. **78**, 1791 (1997).

[6] M. Jamet, W. Wernsdorfer, C. Thirion, D. Mailly, V. Dupuis, P. Mélinon, and A. Pérez, Phys. Rev. Lett. **86**, 4676 (2001).

[7] D. Mailly, C. Chapelier, and A. Benoit, Phys. Rev. Lett. **70**, 2020 (1993).

[8] C. Veauvy, K. Hasselbach, and D. Mailly, Phys. Rev. B **70**, 214513 (2004).

[9] J. Tejada, E. M. Chudnovsky, E. del Barco, J. M. Hernandez, and T. P. Spiller, Nanotechnology **12**, 181 (2001).

[10] S. K. H. Lam and D. L. Tilbrook, Appl. Phys. Lett. **82**, 1078 (2003).

[11] M. B. Ketchen, D. D. Awschalom, W. J. Gallagher, A. W. Kleinsasser, R. L. Sandstrom, J. R. Rozen, and B. Bumble, IEEE Trans. Magn. **25**, 1212 (1989).

[12] L. Hao, J. C. Macfarlane, S. K. H. Lam, C. P. Foley, P. W. Josephs-Franks, and J. C. Gallop, IEEE Trans. Appl. Supercond. **15**, 514 (2005).

[13] P. Anderson and A. H. Dayem, Phys. Rev. Lett. **13**, 195 (1964).

[14] C. D. Tesche and J. Clarke, J. Low Temp. Phys. **29**, 301 (1977).

[15] K. K. Likharev, Rev. Mod. Phys. **51**, 101 (1979).

[16] B. Irmer, R. H. Blick, F. Simmel, W. Godel, H. Lorenz, and J. P. Kotthaus, Appl. Phys. Lett. **73**, 2051 (1998).

[17] V. Bouchiat, M. Faucher, C. Thirion, W. Wernsdorfer, T. Fournier, and B. Pannetier, Appl. Phys. Lett. **79**, 123 (2001).

[18] J. J. A. Baselmans, A. F. Morpurgo, B. J. van Wees, and T. M. Klapwijk, Nature (London) **397**, 43 (1999).

[19] J. Huang, F. Pierre, T. T. Heikkila, F. K. Wilhelm, and N. O. Birge, Phys. Rev. B **66**, 020507(R) (2002).

[20] J. Kutchinsky, R. Taboryski, C. B. Sørensen, J. B. Hansen, and P. E. Lindelof, Phys. Rev. Lett. **83**, 4856 (1999).

[21] T. Schäpers, J. Malindretos, K. Neurohr, S. Lachenmann, A. van der Hart, G. Crecelius, H. Hardtdegen, H. Luth, and A. A. Golubov, Appl. Phys. Lett. **73**, 2348 (1998).

[22] T. Akazaki, H. Takayanagi, J. Nitta, and T. Enoki, Appl. Phys. Lett. **68**, 418 (1996).

[23] H. Takayanagi, T. Akazaki, and J. Nitta, Phys. Rev. Lett. **75**, 3533 (1995).

[24] J. J. A. Baselmans, B. J. van Wees, and T. M. Klapwijk, Appl. Phys. Lett. **79**, 2940 (2001).

[25] J. J. A. Baselmans, B. J. van Wees, and T. M. Klapwijk, Phys. Rev. B **65**, 224513 (2002).

[26] S. B. Lee, D. G. Hasko, and H. Ahmed, Appl. Phys. Lett. **76**, 2295 (2000).

[27] S. B. Lee, D. G. Hasko, and H. Ahmed, Microelectron. Eng. **57-58**, 981 (2001).

[28] S. B. Lee, G. D. Hutchinson, D. A. Williams, D. G. Hasko, and H. Ahmed, Nanotechnology **14**, 188 (2003).

[29] S. B. Lee, G. D. Hutchinson, D. A. Williams, D. G. Hasko, and H. Ahmed, IEEE Trans. Appl. Supercond. **13**, 1104 (2003).

[30] S. B. Lee, Ph.D. thesis, University of Cambridge, 2000.

[31] G. D. Hutchinson, H. Qin, D. G. Hasko, D. J. Kang, and D. A. Williams, Appl. Phys. Lett. **84**, 136 (2004).

[32] G. D. Hutchinson, H. Qin, D. J. Kang, S. B. Lee, D. G. Hasko, M. G. Blamire, and D. A. Williams, Microelectron. Eng. **73-74**, 773 (2004).

[33] W. T. Tsang and T. Vanduzer, J. Appl. Phys. **47**, 2656 (1976).

[34] J. Clarke and J. L. Paterson, Appl. Phys. Lett. **19**, 469 (1971).

[35] G. Testa, C. Granata, C. Calidonna, C. Di Russo, M. Mango Furnari, S. Pagano, M. Russo, and E. Sarnelli, Physica C **368**, 232 (2002).

[36] G. Burnell, E. J. Tarte, D.-J. Kang, R. H. Hadfield, and M. G. Blamire, Physica C **368**, 241 (2002).

[37] K. K. Likharev and L. A. Yakobson, Sov. Phys. Tech. Phys. **20**, 950 (1976).

[38] T. V. Duzer and C. W. Turner, *Principles of Superconductive Devices and Circuits*, 2nd ed. (Prentice-Hall, Englewood Cliffs, NJ, 1999).

[39] W. J. Skocpol, M. R. Beasley, and M. Tinkham, J. Appl. Phys. **45**, 4054 (1974).

[40] G. Bergmann, W. Wei, Y. Zou, and R. M. Mueller, Phys. Rev. B **41**, 7386 (1990).

[41] M. L. Roukes, M. R. Freeman, R. S. Germain, R. C. Richardson, and M. B. Ketchen, Phys. Rev. Lett. **55**, 422 (1985).

[42] N. Perrin, M. N. Wybourne, and J. K. Wigmore, Phys. Rev. B **40**, 8245 (1989).

[43] J. C. Nabity and M. N. Wybourne, J. Phys.: Condens. Matter **2**, 3125 (1990).

[44] W. Little, Can. J. Phys. **37**, 334 (1959).

[45] J. P. Wolfe, *Imaging Phonons: Acoustic Wave Propagation in Solids* (Cambridge University Press, Cambridge, England, 1998).

[46] *CRC Handbook of Tables for Applied Engineering Science*, 2nd ed., edited by R. E. Bolz and G. L. Tuve (CRC Press, Boca Raton, FL, 1973).

[47] G. W. Kaye and T. H. Laby, *Tables of Physical and Chemical Constants*, 16th ed. (Longman Group, Bath, 1995).

[48] T. P. Orlando and K. A. Delin, *Foundations of Applied Superconductivity* (Addison-Wesley, New York, 1991).

[49] M. Tinkham, *Introduction to Superconductivity and High T_C Materials* (World Scientific, Singapore, 1992).

[50] A. Barone and G. Paternò, *Physics and Applications of the Josephson Effect* (Wiley, New York, 1982).

[51] L. G. Aslamazov and A. L. Larkin, JETP Lett. **9**, 87 (1969).

[52] E. de Wolff and R. de Bruyn Ouboter, Physica B **176**, 133 (1992).

[53] K. Hasselbach, D. Mailly, and J. R. Kirtley, J. Appl. Phys. **91**, 4432 (2002).

[54] J. R. Waldram, *Superconductivity of Metals and Cuprates* (Institute of Physics, Bristol, 1996).

[55] M. M. Khapaev, A. Yu. Kidiyarova-Shevchenko, P. Magnelind, and M. Yu. Kupriyanov, IEEE Trans. Appl. Supercond. **11**, 1090 (2001).